Detailed velocity-dependent line shapes for degenerate four-wave mixing spectra in a two-level atomic system

Binh Do
Department of Physics and School of Electrical and Computer Engineering, Purdue University, West Lafayette, Indiana 47907, USA

D. S. Elliott
School of Electrical and Computer Engineering, Purdue University, West Lafayette, Indiana 47907, USA

(Received 15 October 2002; published 19 June 2003)

We study phase-conjugate degenerate four-wave mixing in an optically pumped, two-level atomic system (the $3s^2S_{1/2}$, $F=2$, $m_F=2 \rightarrow 3p^2P_{3/2}$, $F=3$, $m_F=3$ transition in a diffuse, collision-free, thermal beam of sodium). In this investigation, we study the detailed line shape and strength of the four-wave mixing signal as a function of the intensity of the cw pump waves, and of the velocity of the atoms. Our technique allows us to examine the four-wave mixing interaction under conditions in which the Doppler shift, the natural linewidth of the transition, and the Rabi frequency for the interaction are each comparable with one another. From our experimental measurements and computational results, we show that the line shapes are very complex in this regime, and that they depend sensitively upon the atomic velocity, especially in the case when the intensity of the forward and backward pump beams exceeds the saturation intensity for the transition.

DOI: 10.1103/PhysRevA.67.063810 PACS number(s): 42.50.Gy, 32.80.−t, 42.65.Hw

I. INTRODUCTION

Effects of the velocity of atoms in dilute vapors on their interactions with optical fields have been studied over the years in a multitude of interactions. In simple absorption spectra, for example, the atomic velocity results in an inhomogeneous broadening of the absorption spectrum. In general, to resolve narrow spectral features in the laboratory, one must either (1) decrease the range of velocities present in the atomic ensemble (as in atomic beams or systems of trapped atoms) or (2) identify and use an interaction that is essentially free of Doppler broadening effects. One such interaction that has long been known for producing Doppler-free linewidths is phase-conjugate degenerate four-wave mixing (DFWM). It is perhaps surprising, however, that very little attention has been devoted to understanding the detailed dependence of the DFWM interaction on the atomic velocity. The aim of the present work is to explore these atomic velocity effects, and specifically to determine the DFWM line shape and signal strength when the Doppler shift, the natural linewidth of the transition, and the Rabi frequency for the interaction are each comparable with one another.

The DFWM interaction has been employed extensively in various gas, liquid, and solid phase media, and has become a useful tool in numerous applications. One of the more exotic examples of DFWM is optical phase conjugation [1], i.e., the generation of a reflected optical wave whose wave front is matched to that of the incident beam, making possible applications in adaptive optics and image reconstruction [2]. Due to its high sensitivity, DFWM is used to determine the local concentration of species in dilute media [3,4], and its high spectroscopic resolution allows for determination of the rotational and vibrational temperatures of many gaseous media, such as NO [5] or CH [6], and of flames [7–9]. The reflectivity of the DFWM process can be greater than one [10,11], forming the basis for the demonstration of a continuous-wave self-pumped oscillator in an atomic sodium vapor cell [12]. The DFWM has also been used to measure directly the relaxation time of molecular reorientation in a liquid crystal [13], and, in semiconductor media, as a standard tool for measurements of $\chi^{(3)}$ and $\chi^{(5)}$ effects [14,15].

The line shape for phase-conjugate DFWM in gases has been a long-standing problem. Many studies [16–34] over the past two and a half decades have been reported in which the authors have examined the dependence of the DFWM spectrum and the maximum reflectivity on such factors as the intensity of the pump beams [16–18], the asymmetry between the intensity of the forward and backward pump beams [16,19–24], the absorption thickness of the atomic medium [16,25], the inhomogeneous Doppler broadening of the medium [16,18,20–23,26–32], the population redistribution among the various angular momentum components of the lower state [17,25,32], and the bandwidth of the laser [33]. Under differing conditions, spectra consisting of from one to four peaks have been reported.

The importance of atomic motion for four-wave mixing spectra in gas phase media has long been recognized, but an analytic solution for arbitrary velocities and for pump beam intensities exceeding the saturation intensity has not been discovered. It is well known that in the rest frame of an atom, which is moving in the direction of propagation of a laser beam, the apparent frequency of the optical field is lower than the frequency in the laboratory frame. Similarly, an atom moving counter to the direction of propagation of a laser beam feels the optical field at a higher frequency than actual. In phase-conjugate four-wave mixing, the atoms are subjected to two counterpropagating pump fields, so that an atom in motion sees one field Doppler-shifted to a higher frequency and the other shifted to a lower frequency. At low intensities, the atomic response to either of these fields is decreased, and the resulting four-wave mixing amplitude is

small. Only those atoms for which $|\vec{k}\cdot\vec{v}|<\Gamma_0$, where $\vec{k}$ is the propagation vector of the wave, $\vec{v}$ is the atomic velocity, and Γ_0 is the full width at half maximum (FWHM) of the transition, participate in the interaction. For this reason, the signal generated by the phase-conjugate four-wave mixing interaction has been termed ''Doppler free.'' (Doppler free in this context is somewhat different from the same term used for two-photon absorption. In the latter, the Doppler shift of the two laser beams means that for an atom simultaneously absorbing one photon from each of the two counterpropagating laser fields, the sum of the photon energies is independent of the atomic velocity. Therefore, *all* atoms can participate in the Doppler-free two-photon absorption process when the laser frequency is two-photon resonant, producing a narrow-band absorption resonance.) In 1978, Abrams and Lind [16] presented a theory of phase-conjugate DFWM for a two-level atomic system. Their results were valid for arbitrarily high intensities of the forward and backward pump beams, but were limited to stationary atoms. They briefly discussed the role of atomic velocity in this work, but the first detailed treatment to include velocity effects was that of Wandzura [26]. His treatment was reported to be valid for low intensities, and he treated the problem in two extremes: the homogeneously broadened limit (when the natural linewidth is much greater than the Doppler width) and the inhomogeneously broadened limit (when the natural linewidth is much less than the Doppler width). In the low intensity limit considered in this work, Wandzura found that the contribution to the DFWM signal by atoms in motion is always less than that by stationary atoms. He summarized the effect in the homogeneously broadened limit with a velocity-dependent reduction factor for the DFWM reflectivity, and also predicted the DFWM line shape in the inhomogeneously broadened limit.

An experiment by Steel *et al.* [27] provided a test of the Wandzura theory in the homogeneously broadened limit. Using the pulsed 10.6-μm output of a variable pulse duration CO_2 laser, the authors used various combinations of orthogonal polarizations of the three input beams in order to distinguish the different contributions to the DFWM signal. The motion of the molecules in the SF_6 vapor can effectively wash out population or coherence gratings set up in the vapor by its interaction with the input beams, decreasing the magnitude of the four-wave mixing signal. The experimental results of Ref. [27] were consistent with the predictions of Wandzura in this limit. Later experiments by Humphrey *et al.* [28], in which they measured the DFWM spectrum at a variety of crossing angles θ, between the pump and probe beams, were in conflict with Wandzura's predictions. These experimental results showed the linewidth of the DFWM spectrum to be independent of θ, while the theory predicted a linewidth that increased with increasing angle.

Steel *et al.* [29] later reported experiments in which they examined DFWM in a homogeneously broadened SF_6 vapor. They developed a simplistic model for the effect of the molecular velocity, and reported a good agreement between experimental and theoretical results.

A great deal of attention has been devoted to the study of four-wave mixing in the case when one pump beam is strong and the other is weak [20–23]. In this case, it is possible to find an analytic expression for the spectrum as a function of velocity [21], and a very good agreement between measured spectra and theory has been reported for an intense backward pump beam [22,23]. This spectrum exhibits two peaks, separated by a frequency difference in the range of the Rabi frequency of the interaction of the strong pump beam with the atom.

Finally, we recently reported [18] our experimental studies of DFWM with narrow-band cw laser beams in an atomic beam of optically pumped, two-level sodium atoms with equal intensity pump beams, where the intensity of each pump beam exceeds the saturation intensity of the transition. The conditions of these measurements approached those of the fundamental theory presented by Abrams and Lind [16,35]. The influence of atomic velocity on these measurements was highly evident, even in an atomic beam of reasonably good collimation. (The weak-field absorption linewidths for the experimental system were 12.5–14.5 MHz, only slightly greater than the natural linewidth of the D_2 transition in sodium of $\Delta\nu_h=\Gamma_0/2\pi=10$ MHz.) We were able to calculate the contribution of the sodium atoms in motion by numerically integrating the optical Bloch equations, and found an excellent agreement between numerical results and experiment. Analysis of these measurements were limited by atomic velocity redistribution effects (i.e., the distortion of the DFWM spectra due to a deflection of the atomic beam), as we will describe later in this paper.

In the present study, we measure the DFWM spectrum as a function of pump beam intensity and as a function of the atomic velocity. We measure the latter by varying the crossing angle between our laser beams and the atomic beam. We measure the DFWM spectrum as a function of pump beam intensity in a manner similar to our previous work [18], but we have reduced the above-mentioned distortions associated with the deflection of the atomic beam. We use a narrow-band, stabilized, cw tunable dye laser as our source, and an optically pumped beam of atomic sodium as our nonlinear medium in order to minimize other effects that might otherwise mask the effects that we wish to observe. The experimental procedures that we follow allow us to closely match the conditions assumed in the theories by Abrams and Lind [16] and by Wandzura [26], but allow us to examine these effects at intensities exceeding the saturation intensity for the transition, and for atomic velocities leading to Doppler shifts that are comparable to the transition linewidth. We compare the experimental spectra with the results predicted by direct integration of the optical Bloch equations, showing a very close agreement with experimental line shapes as well as signal strengths.

The following sections are organized as follows. We describe the DFWM experiment in Sec. II, and discuss the results and the numerical simulations of DFWM on an atomic sodium beam in Sec. III. We conclude in Sec. IV.

II. EXPERIMENT

In this section, we discuss the experimental techniques that we use for measurements of phase-conjugate four-wave

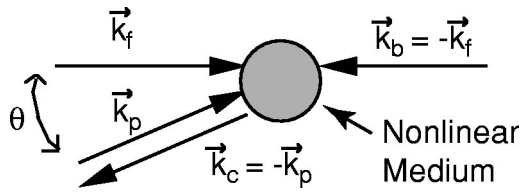

FIG. 1. Wave-vector diagram for the four-wave mixing interaction in the phase-conjugate geometry. Counterpropagating pump beams (propagating in directions $\vec{k}_f$ and $\vec{k}_b = -\vec{k}_f$) and a probe beam ($\vec{k}_p$) interact with the nonlinear medium to produce the phase-conjugate beam ($\vec{k}_c = -\vec{k}_p$).

mixing spectra. Three input beams intersect one another in a nonlinear medium, producing the phase-conjugate beam through their interaction with the medium. We show a schematic representation of the geometry of the input and output beams in Fig. 1. The forward and backward pump beams propagate counter to one another (i.e., $\vec{k}_b = -\vec{k}_f$ where $\vec{k}_f$ and $\vec{k}_b$ are the propagation vectors for the forward and backward pump beams), and cross the atomic beam at close to a right angle. We assign the angle ζ as the deviation of this crossing angle from 90°. A weak probe beam also crosses the atomic beam at the angle ζ, and propagates at a small angle θ with respect to the forward pump beam. All input laser beams are derived from the same laser source, and are at the same frequency. The phase-conjugate beam produced through the DFWM interaction propagates in the direction opposite to that of the input probe beam with $\vec{k}_c = -\vec{k}_p$.

The conditions assumed in our numerical calculations of this interaction and attained in our experiment are (i) the nonlinear medium is a closed, two-level system, (ii) the effect of inhomogeneous broadening in the nonlinear medium is small, and (iii) the nonlinear medium is collision free. To satisfy the first condition, we need to transfer all of the atoms in the atomic beam into a single hyperfine sublevel of the ground ($3s^2S_{1/2}$, $F=2$, $m_F=2$) state before they reach the interaction region. Atoms in the atomic beam still have transverse velocities that are responsible for a small, but nonnegligible, Doppler broadening, so condition (ii) is satisfied. Since the nonlinear medium in this experiment is an atomic beam, condition (iii) is strictly obeyed.

We show a detailed layout of this experiment in Fig. 2. The light source from which all beams are derived is a traveling wave (ring), stabilized, tunable, cw dye laser operating on a Rhodamine 6G jet. We monitor the laser mode with a 2-GHz free spectral range scanning Fabry-Perot interferometer, and tune the laser frequency to within 10 GHz of the D_2 transition using a wave meter (traveling-arm Michelson interferometer) and to within 1.5 GHz by observing the fluorescence from a heated glass sodium vapor cell. The linewidth of the laser field is $\Delta\nu_L \sim 200$ kHz. We drive the acousto-optic modulator (AOM) at a frequency of 200 MHz to deflect and frequency shift a portion of the output of the ring-dye laser, forming what ultimately becomes the three input beams required for the DFWM interaction. As we describe later, we also use this AOM to chop the intensity of the optical beams. The undeflected beam passes through an

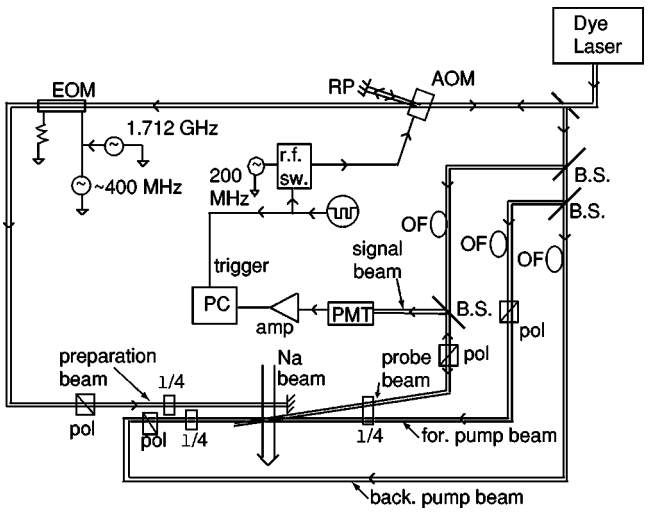

FIG. 2. Schematic diagram for the phase-conjugate four-wave mixing experiment. Abbreviations in this diagram are used for the the acousto-optic modulator (AOM), electro-optic modulator (EOM), a roof prism (RP), a rf switch (rf sw.), optical beam splitters (BS), single-mode optical fibers (OF), the photomultiplier (PMT), a personal computer (PC), polarizers (pol), and quarter-wave retarders ($\lambda/4$).

electro-optic modulator, to which we apply a voltage composed of two sinusoidal components, one at frequency ν_{m1} (tunable in the range 350–450 MHz) and the second at 1.712 GHz. This beam allows us to transfer nearly all the ground-state population of the atomic sodium into a single magnetic component of the ground state, and to control and lock the frequency of the laser, ν_L, in the vicinity of the atomic transition frequency. A side band of this circularly polarized beam at frequency $\nu_L + \nu_{m1}$, resonant with the $3s^2S_{1/2}$, $F=2 \rightarrow 3p^2P_{3/2}$, $F=3$ transition, optically pumps the sodium atoms into a closed, two-level system following the method of Grove, Wu, and Ezekiel [36]. A second-order optical sideband at frequency $\nu_L + \nu_{m1} + 1.712$ GHz is resonant with the $3s^2S_{1/2}$, $F=1 \rightarrow 3p^2P_{3/2}$, $F=2$ transition. This band recovers ground-state atoms from the $3s^2S_{1/2}$, $F=1$ level, allowing them to be active in the DFWM interaction. In order to keep the atoms in the $3s^2S_{1/2}$, $F=2$, $m_F=2$ state as they travel from the preparation region to the interaction region, we cancel the earth's magnetic field and apply an additional static field of magnitude ~ 500 mG, oriented parallel to the direction of propagation of the preparation beam. As is standard for interactions with circularly polarized beams, we choose this direction as the quantization axis of our quantum atomic system, and label this the $\hat{z}$ direction. We collect the fluorescent light emitted from the intersection of this preparation beam and the atomic beam, and generate a correction voltage using the Pound-Drever frequency stabilization method [37,38]. We apply the correction voltage to the ring dye laser frequency control in order to maintain the frequency $\nu_L + \nu_{m1}$ in resonance with the $3s^2S_{1/2}$, $F=2 \rightarrow 3p^2P_{3/2}$, $F=3$ transition.

The laser beam that is deflected by the AOM is reflected back into the AOM (double-pass configuration) to be diffracted a second time. This double-deflected beam is split

into three beams before reaching the atomic beam: the forward pump beam, the backward pump beam, and the probe beam. The frequency of these beams is $\nu = \nu_L + 400$ MHz. Since we lock the frequency of the preparation beam, $\nu_L + \nu_{m1}$, to the frequency ν_{12} of the $3s^2S_{1/2}$, $F=2 \rightarrow 3p^2P_{3/2}$, $F=3$ transition, the detuning of the pump and probe beams from the transition frequency is

$$\Delta/2\pi = (\nu_L + 400 \text{ MHz}) - \nu_{12} = 400 \text{ MHz} - \nu_{m1}. \quad (1)$$

By tuning the frequency ν_{m1}, we indirectly tune the frequency of the pump and probe beams, thus controlling Δ.

In order to equalize the optical path lengths of the pump and probe beams to the atomic beam and to improve their spatial profiles, we pass each of these beams through single-mode optical fibers. The optical path lengths are matched to one another to within less than 1 cm, much less than the optical coherence length ($l_c \sim c/\Delta\nu_L = 1.5$ km) of the laser field. We reduce amplitude fluctuations in the transmitted beams by cutting the input surfaces of the fibers at a slight angle, thus reducing interference effects within the fibers. We further stabilize the probe beam intensity by using an AOM (not shown) and a feedback circuit to control the amplitude of its rf driving voltage.

The laser beams that emerge from the pump beam fibers are collimated by 20× Leica infinity corrected objective lenses (N plan). The laser beam coming out of the probe beam fiber is focused by a 40× objective lens into the AOM of the stabilizing network and then focused into the interaction region by two long focal length (400 mm and 1000 mm) lenses. We correct the polarizations of the collimated beams using half-wave plates before the fibers and polarizers after the fibers. Two quarter-wave plates, one in the path of the forward pump and probe beams and a second in the path of the backward pump beam, convert their polarizations from linear to circular. We vary the power of the forward and backward pump beams from 18 μW to 3.7 mW, and match them to within 2% of each other. The power of the probe beam is fixed at 2 μW. The pump and probe beams are each in a nearly lowest-order Gaussian mode of radius (defined as the radial distance at which the intensity drops to $1/e^2$ of the on-axis intensity) equal to 1.2 mm and 0.28 mm, respectively. We maintain the ratio of these radii so that the intensity of the pump beam is relatively constant (less than 10% variation) over the dimension of the probe beam. The pump beam intensity ranges from 0.13 I_s^0 to 25.4 I_s^0, where I_s^0 is the saturation intensity for the transition at the resonance frequency,

$$I_s^0 = \frac{1}{2}\epsilon_0 c \frac{\hbar^2 \gamma_{12}\Gamma_0}{|\mu_{12}|^2}, \quad (2)$$

where γ_{12} is the transverse relaxation rate and μ_{12} is the transition dipole moment. For the transition used in our work, I_s^0 is 6.33 mW cm^{-2}. The probe beam intensity is $I_{probe} = 0.26\, I_s^0$ for all measurements.

The phase-conjugate beam propagates backward along the direction of the input probe beam. We separate the phase-conjugate and the input probe beams using a nonpolarizing ~30% beam splitter, and direct the former onto the photocathode of a photomultiplier tube [PMT gain $= 1.9\times10^6$, with a 8.5% quantum efficiency]. Alignment of the phase-conjugate beam onto the detector requires special care in that the phase-conjugate beam is weak (less than 0.1 nW of power), and the detection system must discriminate against light scattered by the windows from the relatively intense pump beams. We follow the expected path of the phase-conjugate beam by reflecting the probe beam back onto itself, and reduce the magnitude of the scattered light of the pump beams, which reaches the detector by (i) placing a 1.7 mm diameter aperture in front of the photomultiplier tube and housing the detector inside an opaque enclosure and (ii) making the crossing angle θ between the forward pump beam and the probe beam as large as 1.8°. At this angular separation, the spacing between the centers of the probe and forward pump beams at the window of the vacuum system is 5.5 mm, allowing the spatial aperture in front of the detector to significantly reduce this noise.

The vacuum system is divided into two chambers, one containing the sodium oven and the other the interaction region. We pump these two chambers with a single diffusion pump. When the stainless steel oven is at room temperature, the oven chamber reaches an ultimate pressure of about 3×10^{-7} torr. When we heat the oven, sodium atoms escape through a 1.7-mm-diameter nozzle. An aperture in the chamber wall that separates the oven and interaction chambers, located 367 mm from the oven nozzle, defines the collimated atomic beam in the interaction region. We use two different apertures in this experiment, one of diameter 3.8 mm and the other of 1.7 mm. In order to reduce the number of sodium atoms diffusing into the interaction chamber from the background vapor in the oven chamber, we wrap cold-water copper tubing around the oven chamber to help condense and collect these sodium atoms.

The characterization of the velocity distribution of the atomic beam is important for this study. For atoms in an effusive beam, the average kinetic energy per atom is [39]

$$\left\langle \frac{mv^2}{2} \right\rangle = 2k_B T, \quad (3)$$

where m is the atomic mass, k_B is the Boltzmann constant, and T is the oven temperature. At an oven temperature of 300°C, as we use in our experiment, this yields a root-mean-square velocity of $\langle v \rangle_{rms} = 9.1\times10^4$ cm/sec. The peak of the velocity distribution occurs at $v_{peak} = 7.9\times10^4$ cm/sec.

The atomic beam is also characterized by its distribution of velocities in the direction transverse to the atomic beam axis. This distribution is due to the finite size of the oven nozzle and the atomic beam aperture, and results in a residual Doppler broadening of the absorption spectrum of the sodium atoms even when the crossing angle ζ is zero. We measure absorption spectra of the atomic beam at various crossing angles in order to determine the mean longitudinal velocity $\overline{v_z}$, i.e., the velocity component parallel to $\vec{k}_f$, and the width (FWHM) of the velocity distribution, Δv_z. For

TABLE I. The peak velocity $\overline{v_z}$, the width of the velocity distribution Δv_z, and the Doppler shift $\nu_{12}\overline{v_z}/c$, as a function of crossing angle ζ, as determined from weak-field absorption spectra. These parameters are used to calculate the DFWM spectra shown in Figs. 5 and 6, with the various spectra in these figures identified by the labels in column five. The scaling factors in columns six and seven are the only adjustable parameter used to match theory to the experimental measurements in Figs. 5 and 6, respectively. The $\zeta = 0.0$ data was taken as a separate dataset with a smaller atomic beam aperture from that of the remaining data. The oven temperature and the beam alignment may vary slightly, resulting in a different scaling factor of set (a) from that for sets (b)–(f).

					Scaling factor	
ζ (mrad)	$\overline{v_z}$ (cm/sec)	Δv_z (cm/sec)	$\nu_{12}\overline{v_z}/c$ (MHz)	Figure	$I_{\text{pump}}=16.5\ I_s^0$	$I_{\text{pump}}=6.35\ I_s^0$
0.0	0	620	0	5(a),6(a)	0.98	0.99
0.59	40	705	0.7	5(b),6(b)	0.57	0.94
1.76	115	715	2.0	5(c),6(c)	0.62	0.92
4.10	310	740	5.3	5(d),6(d)	0.65	1.00
8.78	650	820	11.0	5(e),6(e)	0.57	1.03
13.46	1000	940	17.0	5(f), 6(f)	0.61	0.90

each crossing angle, we fit the Doppler-broadened line-shape function to the following form:

$$g(\nu)=\int_{-\infty}^{\infty} P(v_z)g(v_z,\nu)dv_z, \tag{4}$$

where $g(v_z,\nu)$ is the homogeneous absorption spectrum for a particular group of atoms of velocity v_z,

$$g(v_z,\nu)=\frac{\Delta\nu_h}{2\pi[(\nu-\nu_{12}-\nu_{12}v_z/c)^2+(\Delta\nu_h/2)^2]}, \tag{5}$$

and $P(v_z)$ is the velocity distribution function,

$$P(v_z)=\sqrt{\frac{4\ln 2}{\pi}}\frac{1}{\Delta v_z}\exp\left[-4\ln 2\left(\frac{v_z-\overline{v_z}}{\Delta v_z}\right)^2\right]. \tag{6}$$

We determine the peak velocity and the FWHM of the atomic velocity distribution that best fits the calculated absorption spectrum to each measured absorption spectrum. Because of the broad distribution of velocities in the axial direction of the atomic beam, the FWHM of the velocity distribution changes as a function of the crossing angle. We fit $\overline{v_z}$ to a linear function of ζ and Δv_z to a quadratic form, and use these atomic velocities and widths to calculate the four-wave mixing spectra. Values of $\overline{v_z}(\zeta)$ and Δv_z for several angles of ζ are listed in Table I. The former are close to $v_{\text{peak}}\times\zeta$.

The peak amplitude of the weak-field absorption in the interaction region of our atomic beam is 8–9 % when using the 1.7-mm-diameter aperture, and 9–10 % for the 3.8-mm aperture. This corresponds to an attenuation factor, $2\alpha_0 L$, of 0.128 and 0.153 for the two atomic beam apertures, respectively, where α_0 is the field attenuation constant for stationary atoms,

$$\alpha_0=\frac{\pi\nu_L N|\mu_{12}|^2}{c\hbar\epsilon_0\gamma_{12}}, \tag{7}$$

N is the atomic beam density, and L is the absorption length, i.e., the diameter of the atomic beam. Unfortunately, the precision of our measurements of the absorption thickness of the atomic beam is limited, in that it was necessary to modify our apparatus between our measurements of the weak-field absorption and our measurements of the DFWM spectra. Thus, our peak absorption measurements are limited by such factors as the reproducibility of the oven temperature. The attenuation factor that we measure is roughly consistent (within a factor of 2) with our estimate of the product $N\sigma_{\text{abs}}L$, where the atomic beam density is $N=2.8\times10^8$ cm^{-3} and $\sigma_{\text{abs}}=1.66\times10^{-9}$ cm^2 is the absorption cross section.

During the course of these measurements, we determined that the DFWM spectra that we were measuring were highly susceptible to atomic recoil effects as the atoms absorb light from the forward and backward pump beams. To understand this, consider an atom whose velocity has a small component in the $+\hat{z}$ direction (i.e., parallel to $\vec{k}_f$ of the forward pump and counter to that of the backward pump). When the laser frequency is tuned slightly below the transition frequency atoms absorb light from the forward pump beam at a lower rate than they do from the backward pump. The net momentum transferred to atoms, therefore, tends to reduce v_z, and bend the atomic beam to a direction more nearly perpendicular to $\vec{k}$. On the other hand, when the laser is tuned to a frequency greater than the transition frequency, the atoms are more likely to absorb from the forward pump beam, and the momentum transferred to the atoms tends to increase ζ. In the latter case, the beam deflection effect tends to further increase the asymmetry in the rate of absorption from the two laser beams, and the recoil effect is enhanced. For the laser beam dimensions and atomic velocities of our experiment, the atoms spend about 50 lifetimes in the pump beam before they enter the probe beam. Since the atomic velocity

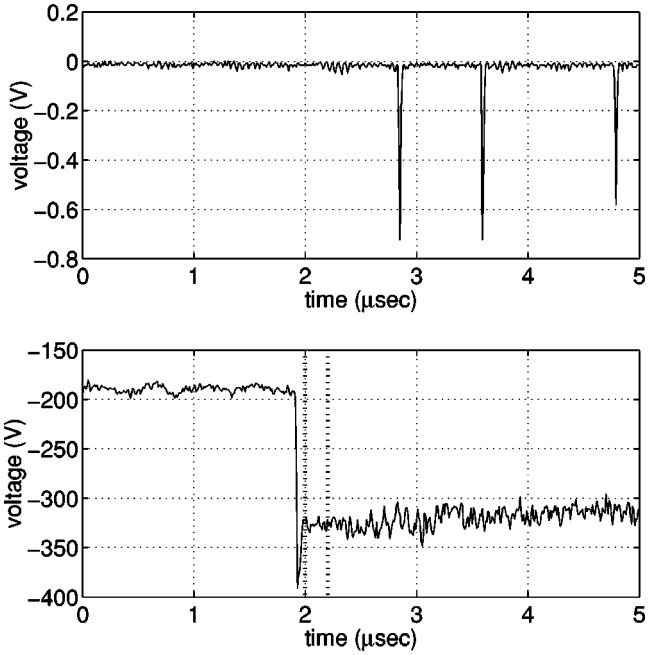

FIG. 3. The oscilloscope trace of the DFWM signal corresponding to (a) a single cycle of the chopped beams, and (b) an accumulation of 10 000 wave forms similar to (a). The pump and probe beams turn on at $t=1900$ nsec. The vertical dashed lines in (b) indicate the time window within which we average to determine the DFWM signal strength.

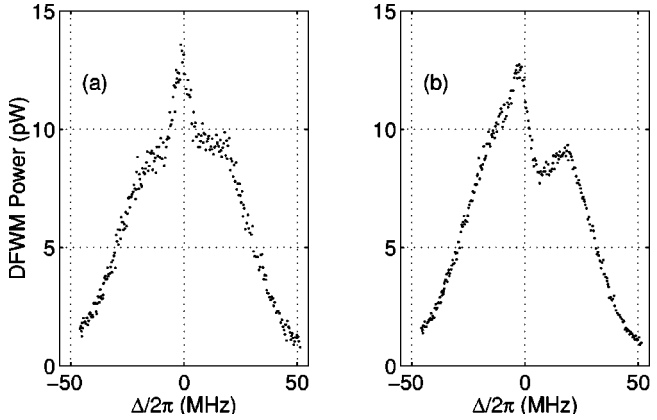

FIG. 4. DFWM spectra at $\zeta=0.0$ and $I_{\mathrm{pump}}=16.5\ I_s^0$, derived from a single series of accumulated wave forms like that shown in Fig. 3(b). The spectrum in (a) was collected in the temporal window between 2.0 and 2.2 μsec, while that shown in (b) used the later window from $t=3.0$ to $t=4.0$ μsec. The distortion of the DFWM spectrum is considerably reduced by chopping the pump and probe beam intensities and limiting our data collection to the 200 nsec window.

distribution can be significantly altered in as few as 10–20 absorption events (v_z changes by 3 cm/sec for each absorption event, with a corresponding Doppler shift of 50 kHz), and the DFWM interaction is very sensitive to the atomic velocity, this recoil effect can significantly distort the DFWM spectra.

As a remedy for this atomic recoil effect, we chop the probe and pump beams by controlling the amplitude of the rf signal that drives the AOM. The period of the cycle is 20 μsec and its duty cycle is 50%. The rise time for the pump and probe beams is $\sim$25 nsec. During the 10 μsec, interval, during which the pump and probe beams are off, the atoms completely traverse the pump beam region. We then repeat the cycle with a fresh group of atoms.

We amplify, display, and record the photomultiplier current with an electronic amplifier (gain=650, input impedance=50Ω, and bandwidth=0–50 MHz) and a digitizing plug-in card [100 MS/s sampling rate, input impedance=50Ω, and bandwidth=0–100 MHz] in a laboratory PC. We show a typical trace of the four-wave mixing signal created for one pulse of the pump and probe beams in Fig. 3(a). The pump and probe beams turn on at about $t=1900$ nsec. At this intensity ($I_{\mathrm{pump}}=16.5I_s^0$) and detuning ($\Delta/2\pi=8.8$ MHz), only three four-wave mixing photons were detected in the period shown. The average integrated area under each photocurrent pulse is about 10.0 V nsec.

We accumulate the DFWM signal by repeating this cycle for 10 000 pulses of the pump and probe beams. We show a typical trace of this accumulated signal in Fig. 3(b). We see an initial transient response in the first 100 nsec after the fields turn on, after which the DFWM signal settles to a relatively constant value. Our numerical simulations, which we will describe later, show that the transient response of the atom is a damped oscillation at a frequency of about 57 MHz. (The Rabi frequency of the Bloch vector due to the interaction of the atom with a *single* pump beam is 28.6 MHz.) When convolved over the 17-nsec duration of a single photoelectron pulse, the computed transient response is similar to that seen between $t=1.9$ μsec and $t=2.0$ μsec in Fig. 3(b). Oscillation of the DFWM signal at the Rabi frequency itself is not observed here, since the photoelectron pulse duration is comparable to the period of oscillation. On a longer time scale of a few microseconds, the signal in Fig. 3(b) shows a 10% decrease. This change is due to the atomic recoil effect, and its magnitude and sign depend upon the detuning of the laser frequency from the transition frequency and on the pump beam intensity. By limiting our data collection to the period from 2.00 to 2.20 μsec on this trace, we reduce the influence of the recoil effect on our DFWM spectra. In Fig. 4, we show two DFWM spectra derived from a single series of accumulated waveforms like those shown in Fig. 3(b). In Fig. 4(a), we used the DFWM signal only within the 200-nsec window, as described. In Fig. 4(b), we used the later DFWM signal from $t=3.0$ μsec until $t=4.0$ μsec. This signal is produced by atoms that have been in the intense pump beams for 1–2 μsec, and the spectrum is therefore distorted by atomic recoil effects. The key signature of this effect is the dip on the high frequency side of the spectrum. One can also observe a slight enhancement of the signal on the low frequency side. All spectra reported in this study are based upon the short (200-nsec) window of integration, and the effects of the atomic recoil are thus minimized.

III. RESULTS AND DISCUSSION

We have measured and recorded degenerate four-wave mixing spectra at a variety of atomic velocities using two

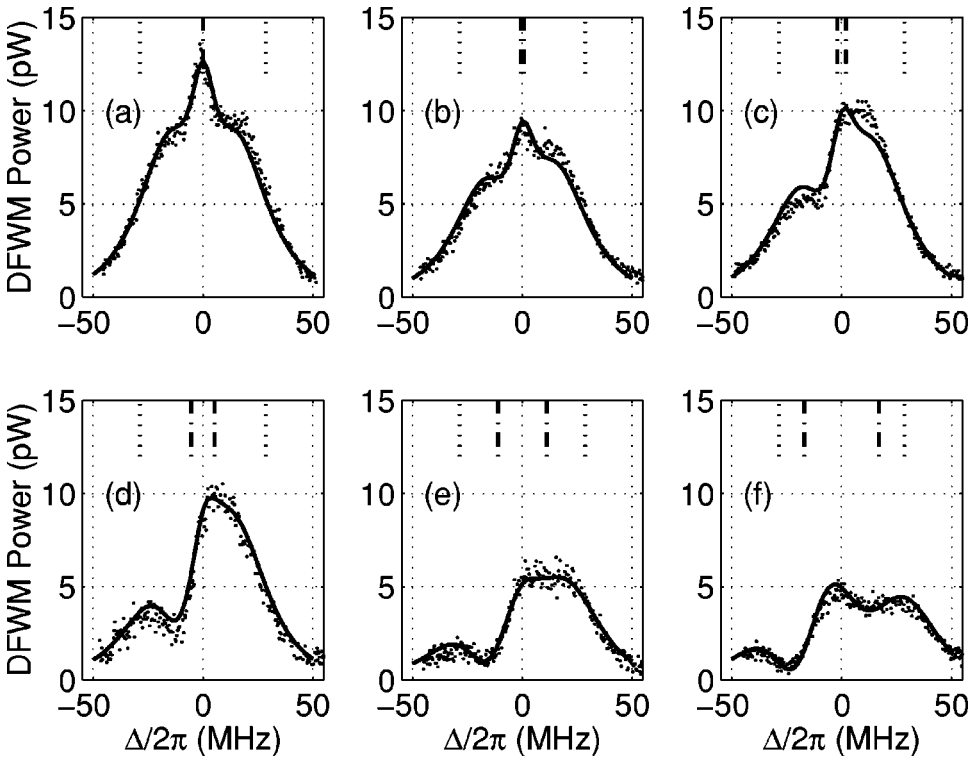

FIG. 5. DFWM spectra at various atomic velocities with $I_{\text{pump}} = 16.5\, I_s^0$. The Rabi frequency at this intensity is 28.6 MHz. The mean Doppler shift due to the atomic velocity, as shown in each figure by the vertical dashed-dot line, is (a) 0 MHz, (b) 0.7 MHz, (c) 2.0 MHz, (d) 5.3 MHz, (e) 11.0 MHz, and (f) 17.0 MHz. See Table I for the crossing angle, mean velocity $\overline{v_z}$, Δv_z, and a multiplicative scaling factor of the order of unity, which produces the best fit of the theory to the experimental spectra for the curves given in these plots.

pump intensity levels, $I_{\text{pump}} = 16.5\, I_s^0$ and $I_{\text{pump}} = 6.35\, I_s^0$. For each crossing angle ζ, we scan the pump and probe frequency from -50 MHz to 50 MHz with respect to the resonance frequency, and record the power of the phase-conjugate beam as a function of the optical frequency. We show the four-wave mixing spectra for six of these measurements at $I_{\text{pump}} = 16.5 I_s^0$ in Fig. 5. The data points in each spectrum represent the experimental measurements, while the solid curve is the result of our computations, to be explained later. We indicate the Rabi frequency due to the interaction of the atoms with one pump beam (28.6 MHz) by vertical dotted lines, and the average Doppler shift, ranging from 0 MHz to 17.0 MHz in our experiment, by the vertical dot dashed lines. We calibrate the optical power of the phase-conjugate beam using an optical power meter and a series of neutral density filters.

In Fig. 5(a), the atomic beam and the probe and pump beams cross each other at 90°, i.e., $\zeta = 0.0$, and the atomic beam aperture diameter is 1.7 mm. The DFWM spectrum is nearly symmetric with respect to the laser detuning from resonance, and has a shoulder on either side of the resonance. The FWHM of the atomic velocity distribution at this angle and beam geometry is $\Delta v_z = 620$ cm/sec, corresponding to a Doppler frequency width of $\nu_{12} \Delta v_z / c = 10.5$ MHz.

The plots shown in Figs. 5(b)–5(f) show the results as we varied the crossing angle of the laser beam and atom beam. In each case shown, $\overline{v_z}$ is positive. Overall we recorded spectra at a total of 12 positive angles and 12 negative angles. We see enhancement of the signal for positive laser detunings, where the Doppler shift effectively tunes the forward pump and probe beams closer to resonance with the transition frequency. Similarly, we observe a dip in the DFWM spectrum corresponding to the detuning at which the backward pump beam is Doppler shifted close to resonance with the transition. The diameters of the oven nozzle and atomic beam aperture are 1.7 mm and 3.8 mm, respectively, for these data, leading to a larger atomic beam divergence than was present for the data shown in Fig. 5(a).

In order to compute the DFWM spectra shown in Fig. 5, we use the theoretical approach described in Ref. [18]. This approach uses the optical Bloch equations to describe the time evolution of the elements of the density matrix ρ of the atomic two-level system. This approach is very similar to that used by Lucht *et al.* [31], except their source was a nanosecond pulsed laser. When the intensity of the probe beam is much less than the saturation intensity for the transition, but that of the pump beams is arbitrary, we can expand the coherence term $\sigma_{21}(\vec{r},t) = \rho_{21}(\vec{r},t) e^{i\omega t}$ and the population probability difference $W(\vec{r},t) = \rho_{22} - \rho_{11}$ in a power series in the phase term of the probe field:

$$\sigma_{21}(\vec{r},t) = \sigma_{21}^{(0)}(\vec{r},t) + \sigma_{21}^{(1)}(\vec{r},t) e^{i\vec{k}_p \cdot (\vec{r} + \vec{v}t)} + \sigma_{21}^{(-1)}(\vec{r},t) e^{-i\vec{k}_p \cdot (\vec{r} + \vec{v}t)},$$

$$W(\vec{r},t) = W^{(0)}(\vec{r},t) + W^{(1)}(\vec{r},t) e^{i\vec{k}_p \cdot (\vec{r} + \vec{v}t)} + W^{(-1)}(\vec{r},t) e^{-i\vec{k}_p \cdot (\vec{r} + \vec{v}t)}. \quad (8)$$

The component $\sigma_{21}^{(-1)}(r,t)$ is the amplitude of the element of the dipole term that radiates the phase-conjugate field. This expansion, after being plugged into the Bloch equations, yields a set of six coupled equations for the coherence and population difference terms,

$$\left(\frac{d}{dt}+\frac{1}{T_2}-i\Delta\right)\sigma_{21}^{(0)}(\vec{r},t)=-i[\Omega\cos(\vec{k}_f\cdot(\vec{r}+\vec{v}t))W^{(0)}(\vec{r},t)+\Omega_p W^{(-1)}(\vec{r},t)/2],$$

$$\left(\frac{d}{dt}+\frac{1}{T_2}-i\Delta\right)\sigma_{21}^{(1)}(\vec{r},t)=-i[\Omega\cos(\vec{k}_f\cdot(\vec{r}+\vec{v}t))W^{(1)}(\vec{r},t)+\Omega_p W^{(0)}(\vec{r},t)/2],$$

$$\left(\frac{d}{dt}+\frac{1}{T_2}-i\Delta\right)\sigma_{21}^{(-1)}(\vec{r},t)=-i\Omega\cos(\vec{k}_f\cdot(\vec{r}+\vec{v}t))\times W^{(-1)}(\vec{r},t),$$

$$\left(\frac{d}{dt}+\frac{1}{T_1}\right)W^{(0)}(\vec{r},t)=i[(2\Omega\cos(\vec{k}_f\cdot(\vec{r}+\vec{v}t))\sigma_{21}^{(0)*}(\vec{r},t)+\Omega_p\sigma_{21}^{(1)*}(\vec{r},t))-(2\Omega^*\cos(\vec{k}_f\cdot(\vec{r}+\vec{v}t))\sigma_{21}^{(0)}(\vec{r},t)+\Omega_p^*\sigma_{21}^{(1)}(\vec{r},t))]-\frac{1}{T_1},$$

$$\left(\frac{d}{dt}+\frac{1}{T_1}\right)W^{(1)}(\vec{r},t)=i[(2\Omega\cos(\vec{k}_f\cdot(\vec{r}+\vec{v}t))\sigma_{21}^{(-1)*}(\vec{r},t)+\Omega_p\sigma_{21}^{(0)*}(\vec{r},t))-2\Omega^*\cos(\vec{k}_f\cdot(\vec{r}+\vec{v}t))\sigma_{21}^{(1)}(\vec{r},t)],$$

$$\left(\frac{d}{dt}+\frac{1}{T_1}\right)W^{(-1)}(\vec{r},t)=i[2\Omega\cos(\vec{k}_f\cdot(\vec{r}+\vec{v}t))\sigma_{21}^{(1)*}(\vec{r},t)-(2\Omega^*\cos(\vec{k}_f\cdot(\vec{r}+\vec{v}t))\sigma_{21}^{(-1)}(\vec{r},t)+\Omega_p^*\sigma_{21}^{(0)}(\vec{r},t))] \quad (9)$$

In these expressions, $\Omega=\vec{\mu}_{21}\cdot\hat{\epsilon}E_f/\hbar$ is the Rabi frequency of the system due to the interaction with a single pump beam, $\Omega_p=\vec{\mu}_{21}\cdot\hat{\epsilon}E_p/\hbar$ is the Rabi frequency of the system due to the probe beam, $T_2=\gamma_{12}^{-1}$ is the coherence lifetime (32 nsec), and $T_1=\Gamma_0^{-1}$ is the population lifetime (16 nsec).

We numerically integrate Eqs. (9), starting with the initial conditions of $W^{(0)}=-1$, and all other terms equal 0, at $t=0$. After a brief transient response due to the fields turning on, each of the coherence amplitudes and population amplitudes settles into a steady-state behavior consisting of a d.c. term and terms oscillating at the frequency $\vec{k}\cdot\vec{v}$ and its harmonics. To compute the phase-conjugate amplitude, we integrate the contribution of all the atoms radiating into this beam throughout the interaction region. Since atoms are distributed evenly throughout the standing wave pattern of the laser beams, the phases of the sinusoidal terms for different atoms are random, and only the d.c. part of $\sigma_{21}^{(-1)}$ contributes to the total DFWM amplitude. We add the complex DFWM field amplitudes computed for different values of the atomic velocity, weighted by the probability distribution of the atomic velocity in the atomic beam, Eq. (6), using values of $\overline{v_z}$ and Δv_z presented in Table I. We calculate the DFWM spectrum using [18]

$$R=\frac{I_c}{I_{\text{probe}}}=\left|2\alpha_0 L\frac{\gamma_{12}}{\Omega_p}\langle\sigma_{21}^{(-1)}\rangle\right|^2, \quad (10)$$

where I_c is the intensity of the conjugate beam. The only parameter that we adjust in order to optimize the agreement of the computed spectra with the measured spectra is a multiplicative scaling factor. We list these factors for the spectra shown in Fig. 5 in column six of Table I. Within the uncertainty in the atomic beam density, this factor is consistent with unity and varies by $\pm 8\%$ over the various spectra within a given dataset [rows (b)–(f) in Table I]. The values of this scaling factor can vary from day to day as the oven temperature and the beam alignment may differ slightly. Since the $\zeta=0$ data was taken as a separate dataset with a smaller atomic beam aperture from that of the remaining data, the difference in the scaling factors for this dataset in comparison with the others is not surprising. The agreement between theoretical and experimental results is very good, with some deviation as observed in Figs. 5(c) or 5(d).

The DFWM spectra that we collected at negative crossing angles, $\zeta<0$, correspond to an atomic velocity that has a positive component in the direction of the backward pump and phase-conjugate signal beams, such that the frequency of these beams is Doppler shifted to the red. Conversely, the frequency of the forward pump and probe beams is blue shifted. A spectrum at a negative angle should be the mirror image of a spectrum of a positive angle scan of the same magnitude, inverted with the respect to $\Delta=0$. In these scans, the pump intensity, the probe intensity, and the sizes of the oven nozzle and atomic beam aperture are each unchanged from the values we used for positive crossing angles. We do not show these spectra here, but the agreement between the theoretical and experimental results is also very good.

We also measured DFWM spectra at the lower pump intensity $I_{\text{pump}}=6.35I_s^0$. We recorded the spectra at a total of 15 crossing angles ζ, including both negative and positive angles. I_{probe} and the diameters of the nozzle and atomic beam aperture have the same values as for the higher intensity measurements. The Rabi frequency for this pump beam intensity is 17.7 MHz. We show six of these spectra, each corresponding to different atomic velocities, in Fig. 6. The agreement between the theoretical and experimental spectra is again uniformly very good. As with the higher intensity spectra, the only adjustable parameter to fit the computed spectra to the measured spectra is another scaling factor, listed in column seven of Table I. These factors vary by $\pm 8\%$ for all of the different spectra we collected in this series [excluding Fig. 6(a) which was part of a different dataset]. The scaling factors for these spectra differ somewhat from those for the higher intensity data, but are consistent within the uncertainty of the atomic beam density. At

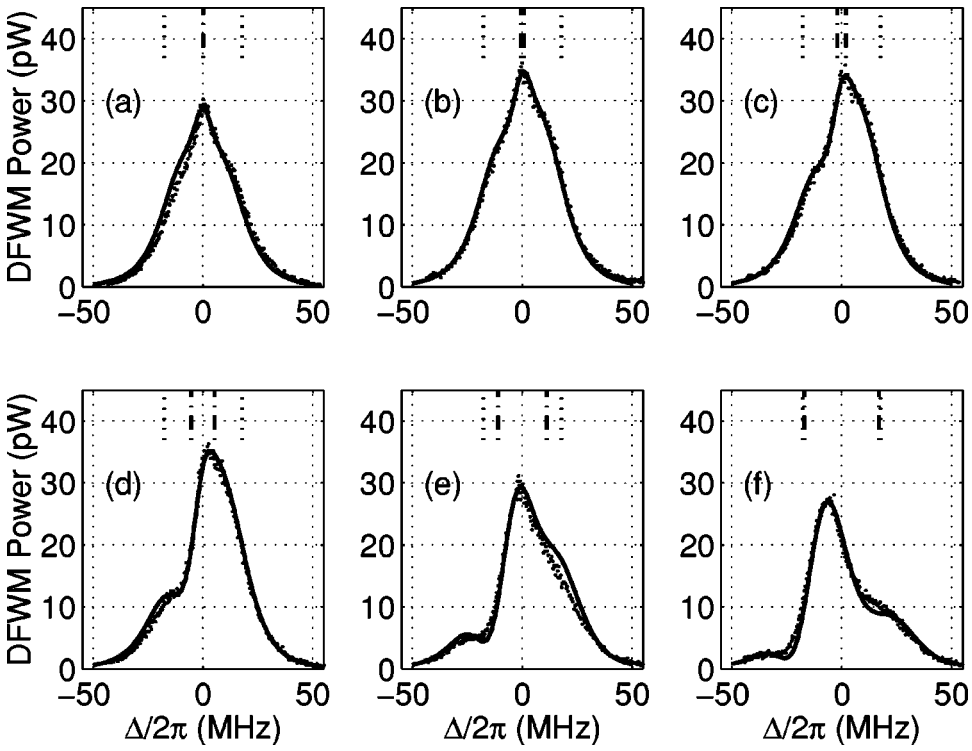

FIG. 6. DFWM spectra at various atomic velocities with $I_{\text{pump}} = 6.35\, I_s^0$. The Rabi frequency at this intensity is 17.7 MHz. The mean Doppler shift due to the atomic velocity, as shown in each figure by the vertical dashed-dot line, is (a) 0 MHz, (b) 0.7 MHz, (c) 2.0 MHz, (d) 5.3 MHz, (e) 11.0 MHz, and (f) 17.0 MHz. See Table I for the crossing angle, mean velocity $\bar{v}_z$, Δv_z, and a multiplicative scaling factor of the order of unity, which produces the best fit of the theory to the experimental spectra for the curves given in these plots.

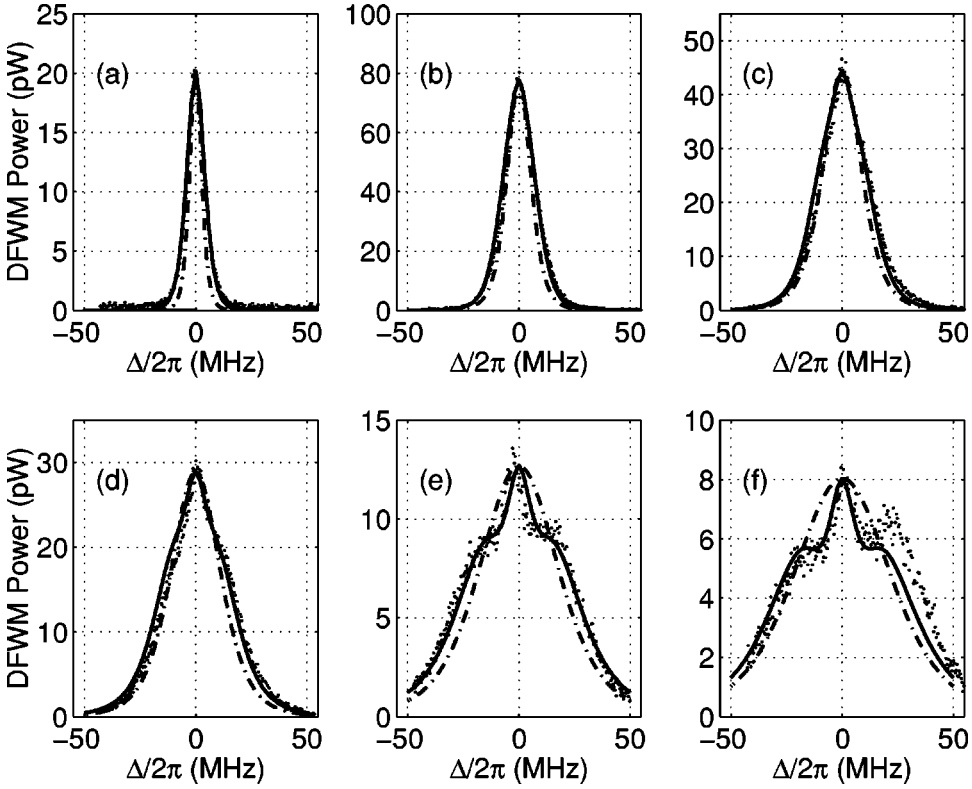

FIG. 7. DFWM spectra illustrating the significance of even a narrow distribution of atomic velocities. The pump intensity is (a) $I_{\text{pump}} = 0.13\, I_s^0$ (b) $I_{\text{pump}} = 1.27\, I_s^0$, (c) $I_{\text{pump}} = 3.81\, I_s^0$, (d) $I_{\text{pump}} = 6.35\, I_s^0$, (e) $I_{\text{pump}} = 16.5\, I_s^0$, and (f) $I_{\text{pump}} = 25.4\, I_s^0$. In each plot, the data points represent the experimental measurements, the solid line represents the computational result based upon a distribution of velocities with $\nu_{12}\Delta v_z/c = 10.5$ MHz, and the dot-dashed line represents the spectrum expected when all atoms are stationary.

this lower pump intensity, the power broadening effect is decreased in comparison with the previous series. The sensitivity of the DFWM spectrum on atomic velocity is also diminished, presumably because we have fewer contributions from the higher velocity atoms to the total four-wave mixing signal.

We have also recorded a series of DFWM spectra as a function of the intensity of the pump beams, taken at right angles (i.e., $\overline{v_z}=0$). In Fig. 7, we show six such spectra with the pump intensity ranging from $I_{\text{pump}}=0.13\ I_s^0$ to $I_{\text{pump}}=25.4\ I_s^0$. In all, we recorded 17 spectra in this range. In these plots, the data points represent the measured DFWM signal, while the lines are computed results. The solid lines are derived from the spectra calculated from Eq. (10), using $2\alpha_0 L=0.124$, and $\langle \sigma_{21}^{(-1)} \rangle$ as determined through numerical integration of Eqs. (9), as described earlier. The mean scaling factor that best fits these computed spectra to the measurements is 1.01, with a standard deviation of 0.05. We use a Gaussian atomic velocity distribution with zero mean and a FWHM of $\Delta v_z=620$ cm/sec, corresponding to the 1.7-mm atomic beam aperture.

We also show in this figure (as the dot-dashed line) the result expected if all atoms were stationary, using [18]

$$R=\left(2\alpha_0 L\frac{I_{\text{pump}}}{I_s^0}\right)^2\left\{\frac{\gamma_{12}^2}{\Delta^2+\gamma_{12}^2(1+4I_{\text{pump}}/I_s^0)}\right\}^3. \quad (11)$$

These zero-velocity spectra are poor fits to the measurements in two respects. (1) The shapes of these computed spectra have no shoulders, and do not agree well with the measured spectra. (2) The amplitudes of the computed spectra are too large, and must be reduced by factors of 2–4 in order to match the peak values of the measurements. The curves clearly show that inclusion of the divergence of the atomic beam is necessary for accurately calculating these DFWM spectra.

In Fig. 8, we show the peak power of the phase-conjugate beam and the linewidth of its spectrum, as determined from plots in Fig. 7 and others like these. The data points indicate the experimental measurements. We also show computed curves for the peak power and linewidth for stationary atoms (dot-dashed line) and for atoms with a distribution of velocities corresponding to our atomic beam (solid line). At each intensity, we computed the peak DFWM signal numerically to produce the solid curve in Fig. 8(a). The stationary-atom result is a plot using Eq. (11). For the plots of the linewidths, the solid line is the result of computing the full spectrum at six different intensities, measuring the linewidth of the computed spectra and fitting a smooth curve to these measurements. The stationary-atom linewidth shown as the dot-dashed line is a plot of the analytic expression [18]

$$\Delta\nu_{FWM}=(\gamma_{12}/\pi)\sqrt{(\sqrt[3]{2}-1)(1+4I_{\text{pump}}/I_s^0)}. \quad (12)$$

The data clearly is better represented by the computations that include the velocity distribution. The peak amplitude data probably fits better than we should reasonably expect, considering the uncertainty in the density of the atomic beam, and thus in $2\alpha_0 L$. The comparison between experimental and theoretical linewidths is unaffected by the uncertainty in $2\alpha_0 L$.

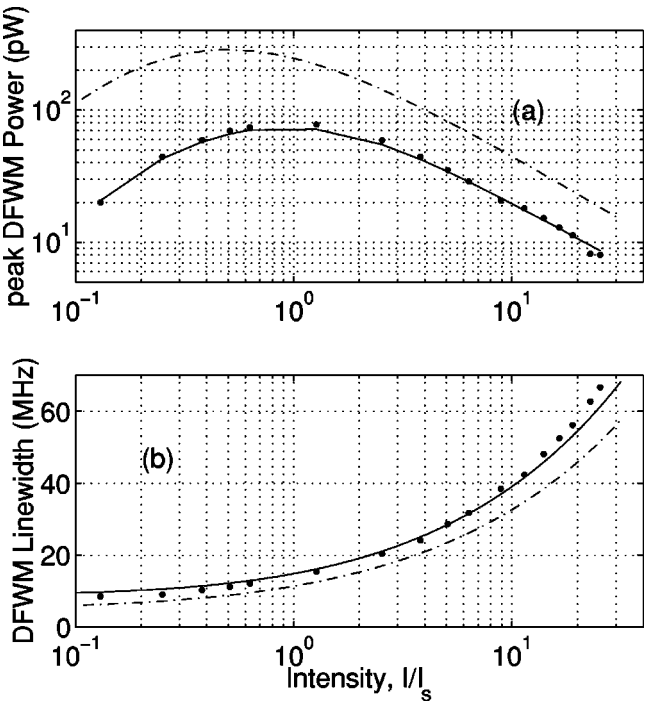

FIG. 8. Peak DFWM power and linewidth (FWHM) of the DFWM spectrum. The experimental measurements are given by the data points, the solid line represents the computed results, including the effects of the atomic motion, and the dot-dash lines are valid for stationary atoms.

We can begin to understand the spectra shown in Figs. 5, 6, and 7 by examining computed DFWM spectra for the different velocity groups that contribute to this signal. In Fig. 9, we show the computed spectra for atoms whose velocity is 0 cm/sec (solid line), 100 cm/sec (dot-dashed line), 300 cm/sec (dashed line), and 500 cm/sec (dotted line), where $I_{\text{pump}}=16.5\ I_s^0$. These velocities correspond to Doppler shifts of 0, 1.7 MHz, 5.1 MHz, and 8.5 MHz, respectively. The spectrum for the zero-velocity atoms is completely symmetric, as expected. As the velocity of the atoms increases, the spectrum becomes asymmetric, and actually becomes narrower and higher than the zero-velocity peak for small positive detunings. The peak DFWM signal corresponds to the case when the forward pump beam is effectively closer to resonance than the backward pump beam (but not *on* resonance). We also note a dip developing on the negative detuning side. The spectrum for the atoms whose velocity is $-v_z$ is the mirror image of the spectrum for the $+v_z$ atoms. At these low velocities, the line shapes are complex and we cannot identify any specific spectral features at $\Delta=\pm|\nu_{12}v_z/c|$. When a distribution of velocities is present, as in our experiment, the enhanced peaks due to these low-velocity atoms combine to give a narrow peak at the center, while the zero-velocity atoms contribute most strongly to the shoulders on the net spectrum, as seen in Fig. 7.

We show a series of computed DFWM spectra for higher velocity atoms in Fig. 10. The pump laser intensity for these

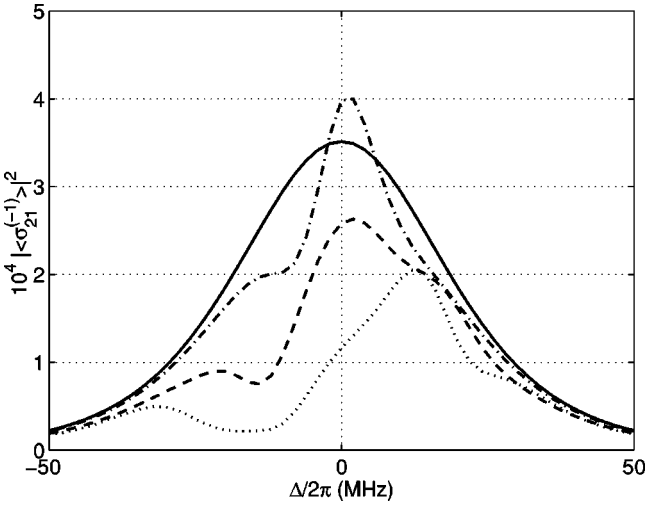

FIG. 9. Computed DFWM spectra for four different atomic velocities: (solid line) 0 cm/sec, (dot-dashed line) 100 cm/sec, (dashed line) 300 cm/sec, and (dotted line) 500 cm/sec. These velocities correspond to Doppler shifts of 0, 1.7 MHz, 5.1 MHz, and 8.5 MHz, respectively. The pump intensity is $I_{\text{pump}}=16.5\ I_s^0$, corresponding to a Rabi frequency of 28.6 MHz.

spectra is $I_{\text{pump}}=16.5\ I_s^0$, as before. The atomic velocities are 1500 cm/sec (solid line), 1800 cm/sec (dot-dashed line), 2200 cm/sec (dashed line), and 3000 cm/sec (dotted line), corresponding to Doppler shifts of 25.4 MHz, 30.6 MHz, 37.4 MHz, and 50.9 MHz, respectively. We are unable to produce laboratory measurements for comparison with these computed spectra, as the geometry of our vacuum apparatus does not allow us to use crossing angles larger than 14 mrad. (The crossing angles required to attain these Doppler shifts, at the peak velocity of our atomic beam, would be 19.0, 22.8, 27.8, and 38.0 mrad, respectively.) Still, these computed

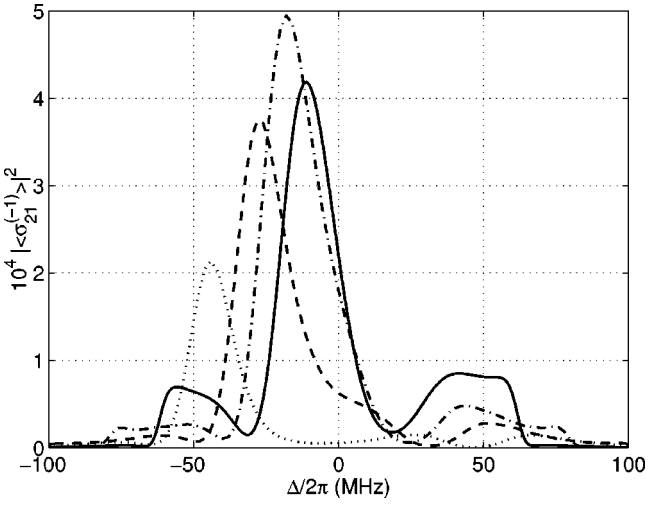

FIG. 10. Computed DFWM spectra for four different atomic velocities: (solid line) 1500 cm/sec, (dot-dashed line) 1800 cm/sec, (dashed line) 2200 cm/sec, and (dotted line) 3000 cm/sec. These velocities correspond to Doppler shifts of 25.4 MHz, 30.6 MHz, 37.4 MHz, and 50.9 MHz, respectively. The pump intensity is $I_{\text{pump}}=16.5\ I_s^0$, corresponding to a Rabi frequency of 28.6 MHz.

spectra are insightful. At these velocities, the Doppler shift exceeds the natural linewidth of the transition (10 MHz), and the spectrum resolves itself into a pair of distinguishable features. The largest feature that we observe in these spectra is a peak at negative detunings (for positive velocity atoms), in contrast to the low-velocity case where the maxima occurred at positive detunings. For Doppler shifts greater than twice the Rabi frequency, this peak occurs at a detuning approaching the Doppler shift, $\Delta\sim-\nu_{12}v_z/c$, and its magnitude decreases with increasing Doppler shift. At this detuning Δ, the effective frequency of the backward pump beam and the phase-conjugate beam is nearly resonant with the transition. This peak becomes especially interesting when the Doppler shift is comparable to the Rabi frequency, as shown by the dot-dashed line in Fig. 10. In this case, the DFWM signal is exceptionally large, and the frequency detuning at which the peak signal occurs (18 MHz) is significantly less than the Doppler shift (30.6 MHz). We believe that this enhancement is likely associated with a resonance between the Doppler-shifted optical frequencies and the transition frequency between dressed states of the atom. Similar effects have been discussed in the context of DFWM with one intense pump beam and one weak pump beam [19–23], for four-wave mixing in self-trapped filaments of light [34], and for nearly degenerate four-wave mixing with two intense pump beams [24]. The dressed states of an atom in a bichromatic laser field were treated theoretically by Agarwal *et al.* [40] in a different context. These authors showed that, in a specialized case, the dressed states of the atom consist of the atomic states with energy ''sidebands'' to either side of the resonance at a frequency spacing of one-half the frequency difference between the two components of the laser field. In the rest frame of the atom, this is the Doppler shift, $\nu_{12}v_z/c$. Another way to picture this system is in the laboratory frame, in which the atom is traveling through the standing-wave pattern of periodicity λ formed by the two counterpropagating pump beams. The atom in the standing wave field is modulated at a frequency v_z/λ (i.e., the Doppler shift), adding energy sidebands at this frequency interval to the atomic internal energy. With the manifold of states introduced by this sideband structure, it becomes plausible that, under the right conditions, the frequencies $\Delta-\nu_{12}v_z/c$ and $\Delta+\nu_{12}v_z/c$ are simultaneously resonant with transitions between internal states and sidebands. From our computed spectra, it appears that the condition for this is that the Doppler shift is comparable to the Rabi frequency. An analytic treatment of this interaction would aid greatly in the interpretation of these results.

Another way to visualize the enhancement that we observe when the Doppler shift is close to the Rabi frequency is presented in Fig. 11, where we plot the maximum four-wave mixing signal strength computed as a function of the atomic velocity when the intensity of the pump beam is $I_{\text{pump}}=16.5\ I_s^0$, with a corresponding Rabi frequency of 28.6 MHz. The peak contribution to the signal is by atoms whose velocity is 1780 cm/sec, corresponding to a Doppler shift of 30.2 MHz. Secondary peaks at velocities corresponding to Doppler shifts of 20.5 MHz, 10.2 MHz, and 1.7 MHz are also observable in this figure. We have computed similar

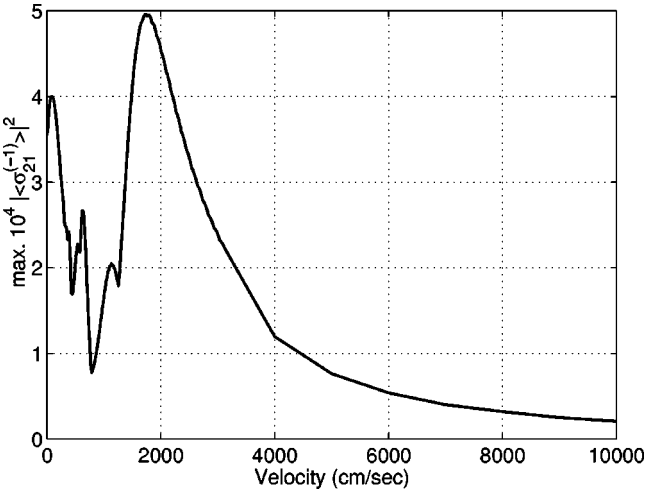

FIG. 11. The maximum DFWM signal strength vs atomic velocity. The intensity of the pump beam for this plot is $I_{\text{pump}} = 16.5\ I_s^0$, with the Rabi frequency at this intensity is 28.6 MHz. The peak contribution to the signal is by atoms whose velocity is 1780 cm/sec, corresponding to a Doppler shift of 30.2 MHz.

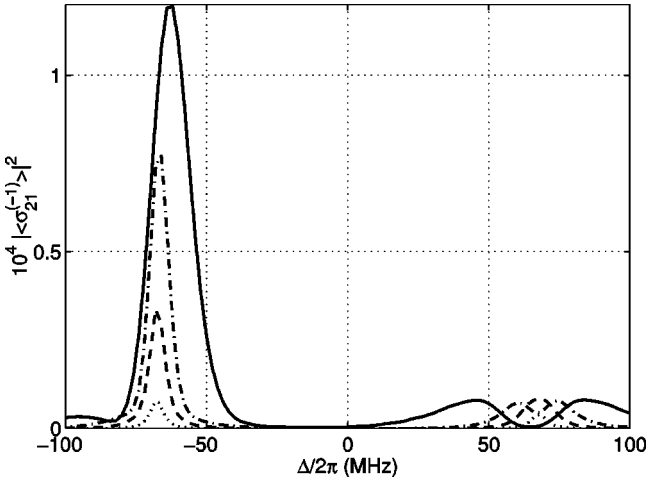

FIG. 12. DFWM spectra for four different pump laser intensities. The Doppler shift is 67.9 MHz for each. The pump intensity is (solid line) $I_{\text{pump}} = 16.5\ I_s^0$, (dot-dashed line) $I_{\text{pump}} = 3.16\ I_s^0$, (dashed line) $I_{\text{pump}} = 1.0\ I_s^0$, and (dotted line) $I_{\text{pump}} = 0.25\ I_s^0$.

curves at lower intensities, and observe the signal enhancement when the Doppler shift and the Rabi frequency are nearly equal in each case. The frequency at which this maximum signal appears is a function of the pump beam intensity.

Finally, we plot in Fig. 12 several DFWM spectra at different intensities of the pump beam. The velocity of the atoms in each curve is 4000 cm/sec, corresponding to a Doppler shift of 67.9 MHz. The pump beam intensity for each line is $I_{\text{pump}} = 16.5\ I_s^0$ (solid line), $I_{\text{pump}} = 3.16\ I_s^0$ (dot-dashed line), $I_{\text{pump}} = 1.0\ I_s^0$ (dashed line), and $I_{\text{pump}} = 0.25\ I_s^0$ (dotted line). For each of these spectra, the Doppler shift is greater than the Rabi frequency (28.5 MHz, 12.6 MHz, 7.1 MHz, and 0.4 MHz, for the four intensities, respectively). The spectrum for the highest pump intensity shows a large maximum near $\Delta = -\nu_{12} v_z/c$ and a smaller feature with the dip in the center near $\Delta = +\nu_{12} v_z/c$. As the intensity of the pump is decreased, however, the magnitude of the peak near $\Delta = -\nu_{12} v_z/c$ decreases monotonically, and its peak frequency shifts closer to $-\nu_{12} v_z/c$, presumably because the dressed state energies asymptotically approach the bare atom energies. The shape of the feature at $\Delta = +\nu_{12} v_z/c$ changes significantly, approaching a single peaked structure, but retains nearly the same amplitude. At the lowest pump intensity shown in this figure, the peaks at $\Delta = \pm \nu_{12} v_z/c$ are nearly of the same shape, but differ in magnitude by a factor of 2. This low intensity spectrum can be justified in a third-order perturbation picture, in which the DFWM signal is enhanced by a resonance with the backward pump and signal beams at $\Delta = -\nu_{12} v_z/c$, and to a lesser degree, a resonance with the forward pump and probe beams at $\Delta = +\nu_{12} v_z/c$.

IV. CONCLUSIONS

We have studied detailed line shapes for DFWM spectra in a two-level atomic system. In particular, we have examined the dependence of the phase-conjugate signal on pump beam intensity and atomic velocity for the case when the intensities of the two pump beams are equal, and they exceed the saturation intensity. In our studies, the Doppler shift, the Rabi frequency, and the natural linewidth of the transition are all comparable with one another. Agreement between measured spectra and numerical results is very good.

For Doppler shifts smaller than or comparable to the natural linewidth of the transition, and for pump beam intensities greater than the saturation intensity, we show, through experiments and numerical results, that the DFWM line shapes are very complex, and that the maximum DFWM signal occurs for detunings such that the Doppler-shifted frequency of the forward pump beam is closer to resonance than that of the backward pump beam. These line shapes vary rapidly with changes in the atomic velocity. Our numerical results tell us that at larger Doppler shifts, the DFWM spectrum reduces to two spectral features, a large peak when the backward pump beam is near resonance, and a smaller, more complex feature, when the forward pump beam is near resonance. The velocity of the atoms that contribute most strongly to the DFWM signal corresponds to a Doppler shift that is close to the pump Rabi frequency for the interaction. This suggests that resonances of all four beams with transitions between dressed states of the system may play an important role. While our numerical DFWM spectra based upon the optical Bloch equations are in an excellent agreement with our experimental results, an analytic treatment of this problem would clearly help in interpretation of the spectra and in understanding the role of dressed state resonances.

ACKNOWLEDGMENTS

This material is based upon work supported in part by the U.S. Army Research Office under Grant No. DAAH04-95-1-0361. We are also grateful for useful discussions with Arthur Mills and technical assistance from Bryan Winningham and Barrett Robinson during the course of these measurements.

[1] T.R. O'Meara, D.M. Pepper, and J.O. White, in *Optical Phase Conjugation*, edited by Robert A. Fisher (Academic Press, San Diego, 1983), Chap. 14.
[2] D.M. Bloom and G.C. Bjorklund, Appl. Phys. Lett. **31**, 592 (1977).
[3] B.A. Mann, R.F. White, and R.J.S. Morrison, Appl. Opt. **35**, 475 (1996).
[4] T.A. Reichardt, W.C. Giancola, C.M. Shappert, and R.P. Lucht, Appl. Opt. **38**, 6951 (1999).
[5] R.L. Farrow, D.J. Rakestraw, and T. Dreier, J. Opt. Soc. Am. B **9**, 1770 (1992).
[6] S. Williams, D.S. Green, S. Sethuraman, and R.N. Zare, J. Am. Chem. Soc. **114**, 9122 (1992).
[7] C.F. Kaminski, I.G. Hughes, G. M Lloyd, and P. Ewart, Appl. Phys. B: Lasers Opt. **62**, 39 (1996).
[8] P. Ewart and P. Snowdon, Opt. Lett. **15**, 1403 (1990).
[9] V. Sick, M.N. Bui-Pham, and R.L. Farrow, Opt. Lett. **20**, 2036 (1995).
[10] P.J. Saon, A.D. Case, M.J. Damzen, and M.H.R. Hutchinson, Opt. Lett. **17**, 781 (1992).
[11] D.M. Bloom, P.F. Liao, and N.P. Economou, Opt. Lett. **2**, 58 (1978).
[12] C.J. Gaeta, J.F. Lam, and R.C. Lind, Opt. Lett. **14**, 245 (1989).
[13] Ye Peixuan, Chu Guiyin, Zhang Zhiguo, Fu Panming, J. Guoshu, and Lin Xi, Sci. Sin. **24**, 761 (1981).
[14] E.J. Canto-Said, D.J. Hagan, and Eric W. van Stryland, IEEE J. Quantum Electron. **27**, 2274 (1991).
[15] K.S. Bindra, S.M. Oak, and K.C. Rustagi, Phys. Rev. B **59**, 2968 (1999).
[16] R.L. Abrams and R.C. Lind, Opt. Lett. **2**, 94 (1978); **3**, 205 (1978).
[17] P.F. Liao, D.M. Bloom, and N.P. Economou, Appl. Phys. Lett. **32**, 813 (1978).
[18] Binh Do, Jongwhan Cha, D.S. Elliott, and S.J. Smith, Phys. Rev. A **58**, 3089 (1998).
[19] D. Bloch, R.K. Raj, K.S. Peng, and M. Ducloy, Phys. Rev. Lett. **49**, 719 (1982).
[20] G. Grynberg, M. Pinard, and P. Verkerk, Opt. Commun. **50**, 261 (1984).
[21] M. Ducloy, F.A.M. de Oliveira, and D. Bloch, Phys. Rev. A **32**, 1614 (1985).
[22] P. Verkerk, M. Pinard, and G. Grynberg, Phys. Rev. A **34**, 4008 (1986).
[23] M. Pinard, P. Verkerk, and G. Grynberg, Phys. Rev. A **35**, 4679 (1987).
[24] J. Lin, A.I. Rubiera, and Y. Zhu, Phys. Rev. A **52**, 4882 (1995).
[25] M. Oria, D. Bloch, M. Fichet, and M. Ducloy, Opt. Lett. **14**, 1082 (1989).
[26] S.M. Wandzura, Opt. Lett. **4**, 208 (1979).
[27] D.G. Steel, R.C. Lind, J.F. Lam, and C.R. Guiliano, Appl. Phys. Lett. **35**, 376 (1979).
[28] L.M. Humphrey, J.P. Gordon, and P.F. Liao, Opt. Lett. **5**, 56 (1980).
[29] D.G. Steel and J.F. Lam, Opt. Commun. **40**, 77 (1981).
[30] P.R. Berman, D.G. Steel, G. Khitrova, and J. Liu, Phys. Rev. A **38**, 252 (1988).
[31] R.P. Lucht, R.L. Farrow, and D.J. Rakestraw, J. Opt. Soc. Am. B **10**, 1508 (1993).
[32] D.S. Glassner, B. Ai, and R.J. Knize, Opt. Lett. **19**, 2071 (1994).
[33] Binh Do, Jongwhan Cha, D.S. Elliott, and S.J. Smith, Phys. Rev. A **60**, 508 (1999).
[34] D.J. Harter and R.W. Boyd, Phys. Rev. A **29**, 739 (1984).
[35] R.L. Abrams, J.F. Lam, R.C. Lind, D.G. Steel, and P.F. Liao, in *Optical Phase Conjugation*, edited by Robert A. Fisher (Academic Press, San Diego, 1983), Chap. 8.
[36] R.E. Grove, F.Y. Wu, and S. Ezekiel, Phys. Rev. A **15**, 227 (1977).
[37] R.V. Pound, Rev. Sci. Instrum. **17**, 490 (1946).
[38] R.W.P. Drever, J.L. Hall, F.V. Kowalski, J. Hough, G.M. Ford, A.J. Munley, and H. Ward, Appl. Phys. B: Photophys. Laser Chem. **31**, 97 (1983).
[39] R. Pathria, *Statistical Mechanics* (Permagon Press, Oxford, 1972), p. 149.
[40] G.S. Agarwal, Yifu Zhu, Daniel J. Gauthier, and T.W. Mossberg, J. Opt. Soc. Am. B **8**, 1163 (1991).